Crustal structure of western Hispaniola (Haiti) from a teleseismic receiver function study

Jordane Corbeau, Frédérique Rolandone, Sylvie Leroy, K. Guerrier, D. Keir, G. Stuart, V. Clouard, R. Gallacher, S. Ulysse, D. Boisson, et al.

Crustal structure of western Hispaniola (Haiti) from a teleseismic receiver function study

Corbeau J.[1,2], Rolandone F.[1], Leroy S.[1], Guerrier K.[3], Keir D.[4,5], Stuart G.[6], Clouard V.[2], Gallacher R.[4], Ulysse S.[3], Boisson D.[3], Bien-aimé Momplaisir R.[3], Saint Preux F.[7], Prépetit C.[7], Saurel J-M.[2], Mercier de Lépinay B.[8] and Meyer B.[1]

[1]Sorbonne Universités, UPMC Univ Paris 06, CNRS, Institut des Sciences de la Terre de Paris (ISTeP), 4 place Jussieu, 75005 Paris, France

[2]Now at Observatoire Volcanologique et Sismologique de Martinique (OVSM), Institut de Physique du Globe de Paris (IPGP), UMR 7154, CNRS Sorbonne Paris Cité, Paris, France

[3]URGeo, Faculté des Sciences, Université d'Etat d'Haiti, Port-au-Prince, Haiti

[4]Ocean and Earth Science, National Oceanography Center Southampton, University of Southampton, Southampton, SO14 3ZH, UK

[5] Dipartimento di Scienze della Terra, Universita degli Studi di Firenze, Florence 50121, Italy

[6] Institute of Geophysics and Tectonics, School of Earth and Environment, University of Leeds, Leeds, LS2 9JT, UK

[7] Bureau des Mines et de l'Energie, Unité Technique de Sismologie, Port-au-Prince, Haiti

[8] Université Côte d'Azur, CNRS/IRD/OCA, Géoazur, Valbonne, France

Corresponding author: Jordane Corbeau, corbeau@ipgp.fr

Abstract

Haiti, located at the northern Caribbean plate boundary, records a geological history of terrane accretion from Cretaceous island arc formations to the Eocene to Recent oblique collision with the Bahamas platform. Little is presently known about the underlying crustal structure of the island. We analyze P-waveforms arriving at 27 temporary broadband seismic stations deployed over a distance of 200 km across the major terrane boundaries in Haiti to determine the crustal structure of western Hispaniola. We compute teleseismic receiver functions using the Extended-Time Multi-Taper method and determine crustal thickness and bulk composition (V_P/V_S) using the H-k stacking method. Three distinctive and fault-bounded crustal domains, defined by their characteristic Moho depth distributions and bulk crustal V_P/V_S, are imaged across Haiti. We relate these domains to three crustal terranes that have been accreted along the plate boundary during the northeastwards displacement of the Caribbean plate and are presently being deformed in a localized fold and thrust belt. In the northern domain, made up of volcanic arc facies, the crust has a thickness of ~23 km and Vp/Vs of 1.75 +/- 0.1 typical of average continental crust. The crust in the southern domain is part of the Caribbean Large Igneous Province (Caribbean LIP), and is ~22 km thick with Vp/Vs of 1.80 +/- 0.03 consistent with plume-related rocks of late Cretaceous age. Significantly thicker, the crust in central Haiti has values of Moho depths averaging ~41 km and with Vp/Vs of 1.80 +/- 0.05. We propose that the central domain is likely constructed of an island arc upper crust with fragments of dense material originating from mafic lavas or LIP material. We produce a crustal profile along a N-S transect across Haiti accounting for the surface geology, shallow structural history, and new seismological constraints provided by variations of crustal thickness and bulk composition.

Keywords: Receivers Function, Haiti, crustal structure

1- Introduction

1.1- Overview

One of the keys to understanding the transpressive northern Caribbean plate boundary and its geodynamic evolution is constraining crustal thickness and composition. Several geological field studies have led to a description of the shallow structure and stratigraphy of the island of Hispaniola (e.g., Mann et al., 1995; Pubellier et al., 2000). The M_w 7.0 2010 Haiti earthquake prompted several geological and geophysical studies to constrain the fault geometry and the crustal structure in the area of the mainshock (e.g., Douilly et al., 2013). However, our knowledge of the mid- and lower-crustal tectonics remains very limited in the absence of whole crustal geophysical studies in Haiti. In Dominican Republic, the eastern part of Hispaniola Island, interpretation of crustal thickness from gravity data shows thick crust below the southern flank of the Dominican Central Cordillera (Bowin, 1976). From April 2013 for nearly 14 months, a temporary seismic network consisting of 27 stations was deployed in Haiti (Trans-Haiti project) to determine its crustal thickness and bulk composition using teleseismic P-wave data. In addition, we analyze seismograms from 3 permanent stations of the Canadian National network (2010-2015) operated by the Bureau des Mines et de l'Energie and UTS. This paper is the first one about works on temporary deployment of seismometers cross-cutting the whole of the island.

The purpose of the present study is to determine crustal structure across Haiti from receiver function (RF) analysis below Haiti so as to better constrain plate scale tectonic evolution of the region responsible for the development of the current fold−thrust belt (Mann et al., 1995; Pubellier et al., 2000; Hernaiz Huerta et al., 2007). The receiver function analysis technique is an appropriate approach to image major discontinuities within the crust and upper mantle from incoming teleseismic P-waveforms (e.g. Ammon, 1991).

1.2- Geological and tectonic setting of Haiti

Haiti, the western part of the Hispaniola island, is located on the Northern Caribbean plate boundary, which separates the Caribbean plate from the North American plate (Fig. 1). Currently, the Caribbean plate moves in a east-northeast direction at about 20 mm/yr relative to the North American plate (Symithe et al., 2015). As the plate boundary is oriented E-W and the displacement vector of the Caribbean plate is about N70°, the area undergoes oblique collision and transpression at a large restraining bend in the strike−slip plate boundary. The deformation of the Northern Caribbean plate boundary in Haiti is partitioned and two major E-W left-lateral strike-slip faults, the Septentrional-Oriente Fault Zone (SOFZ) in the North and the Enriquillo-Plantain-Garden Fault Zone (EPGFZ) in the south with both faults accommodating the strike-slip component of the displacement (Fig. 1). GPS geodesy shows that compression is mainly accommodated by Miocene to recent folding and thrusting in the North−Haitian thrust fault and the Massif de la Selle in southern Haiti (Symithe and Calais, 2016). The Trans-Haitian fold-and-thrust belt in central Haiti (Fig. 1) was active until the late Neogene (Mann et al., 1995) but does not

appear to accommodate significant shortening today.

The geological and geodynamical history of Haiti is complex, however, two distinct domains have been identified. Haiti is part of the Cretaceous volcanic island arc constituted at the boundary of the Pacific realm (Pindell et al., 2006) called the Greater Antilles arc. The Greater Antilles volcanic arc was initiated by an eastward dipping subduction in Central America (Pindell et al., 2012; Van der Lelij, 2013; Hastie *et al.*, 2013). The Greater Antilles arc now consists of a part of Cuba, Hispaniola and Puerto Rico islands (Mann et al., 1995). This island arc constitutes two thirds of Hispaniola Island, and is mainly made up of arc magmatic facies (Boisson, 1987; Escuder Viruete et al., 2006). The southern part of Haiti has been interpreted to be part of the Caribbean Large Igneous Province (LIP), formed during the Cretaceous on the Pacific Farallon plate, over the Galapagos hotspot (Duncan and Hargraves, 1984). The LIP outcrops as a tholeitic substratum associated with Upper Cretaceous sediments in the Southern Peninsula of Haiti (Calmus, 1983), and has been imaged south and west of Haiti with refraction and reflection data (Leroy et al., 2000; Mauffret et al., 2001; Corbeau et al., 2016a). The volcanic island arc and the LIP subsequently moved north- and eastwards from their Pacific position between the North and South American plates, thus partitioning the current Caribbean plate (Pindell, 2012). The Greater Antilles arc became an inactive intra-oceanic arc at the end of the Upper Cretaceous when it collided with the Bahamas carbonate platform (Leroy et al., 2000; Cruz-Orosa et al., 2012; Iturralde-Vinent et al., 2006). Between the island arc and the LIP lies the Quaternary Cul-de-Sac sedimentary basin (Fig. 1), which is bounded to the North by the thrusts of the Trans-Haitian belt, also called Haiti fold and thrust belt. This belt is formed of NW-SE thrusts having propagated towards the SW since the Lower Miocene (Pubellier et

al., 2000).

1.3- Previous geophysical work

Previous geophysical studies have placed crude constraints on crustal structure in the south and in the vicinity of Haiti that help place our results in context and aid interpretation.

A compilation of seismic refraction data acquired in the Caribbean plate shows that the thickness of the crust is not uniform (Diebold et al., 1981; Mauffret and Leroy, 1997; Mauffret et al., 2001). The Caribbean oceanic crust is 5-km thick in Haitian sub-basin, Colombia and Venezuela basins (Fig. 1). In the middle of the Caribbean plate, the original oceanic crust is underplated by ultra-mafic material (Leroy et al., 2000), forming a LIP of ~10 to 15 km in thickness. The Beata Ridge (Fig. 1), 20-30 km thick, is composed of oceanic crust underplated by an ~15-20 km higher velocity (6 to 8 km/s) ultra-mafic magmatic material and covered by a thin volcanic layer of ~2 km (basaltic with a P-wave velocity of 4.5 to 6 km/s). Submersible sampling along the Beata Ridge to the South of Haiti (Mauffret et al., 2001) confirmed the deep origin of the underplated materials that are ultra-mafic rocks such as picrites or komatiites (Revillon et al., 2000).

In addition, Douilly et al. (2013) provide a velocity model for the crust in the southern part of Haiti, and show that the mean Vp/Vs in this area is 1.80, which is typical for oceanic crust mafic rocks (Christensen, 1996). Velocity model and receiver functions studies made by Moreno et al. (2002) and Gonzalez et al. (2012) show that the depth of the Moho is approximately 20 km in the south of Cuba. In eastern Hispaniola, a seismic refraction study shows that the Moho is at approximately 24 km depth, and reaches roughly

30 km deep in the central part of Hispaniola (Nuñez et al., 2015). The S- and Lg-wave study of McNamara et al. (2012) implies that the Moho in the southwestern part of Hispaniola is 20.6 km depth.

2- Data and Method

2.1- Data

We use data from the 27 broadband stations of the temporary Trans-Haiti network deployment (April 2013 – June 2014), spanning Haiti from North to South (Fig. 2). This unique data set used SEIS-UK and iSTeP UPMC instruments that included 15 CMG-40TD and 12 CMG-6TD seismometers (30s natural period, 100 sps sampling rate). Additionally, we use data from 3 broadband permanent stations of the Canadian National Seismic network installed in Haiti after the 2010 Mw 7.0 earthquake and co-operated by the Bureau des Mines et de l'Energie – UTS (Fig. 2).

To construct receiver functions we use seismograms from teleseismic earthquakes of magnitudes Mw > 5.0, with epicentral distances between 30° and 90°. The initial data set includes a total of 580 events recorded by the Trans-Haiti stations between April 2013 and June 2014, and 2473 events for the Canadian stations between February 2010 and August 2015. The data are generally noisy, due to cultural noise sources, and a second order Butterworth filter with corner frequencies of 0.03 and 2 Hz is applied to the data prior to analysis. A visual quality control is subsequently performed on all the data such that only seismograms that have clear direct-P arrivals are used to produce receiver functions. This results in a reduced data set of 149 event records, with a range of between 2 and 13 per station. A map showing the epicentral distribution of the analyzed earthquakes is given in

139 Fig. 3. Note that the majority of the events arrive from the south of the seismic network.

140

141 **2.2- Receiver function technique**

142 To image the crustal structure beneath Haiti we use the receiver function (RF)
143 method (e.g. Ammon, 1991), which is a deconvolution technique for isolating the P-to-S
144 converted phases (Ps) and associated reverberations (PpPs and PsPs + PpSs) of an incoming
145 P-waveform beneath a seismic station. The incident P-wave on the vertical component is
146 deconvolved from the radial and tangential components to remove source complexity and
147 leave a series of pulses that represent the P-to-S phase conversions (the so-called receiver
148 function).

149 Several deconvolution methods have been developed with different noise
150 stabilization processes: deconvolution in the frequency domain (Langston, 1979; Owens et
151 al., 1983; Ammon, 1991); deconvolution in the time domain by least squares estimation
152 (Abers et al., 1995); iterative deconvolution in the time domain (Gurrola et al., 1995;
153 Ligorria and Ammon, 1999) and multi-taper frequency domain cross-correlation (MTRF)
154 (Park and Levin, 2000; Helffrich, 2006). The advantage of the last method is that it works
155 on the correlated signal and mitigates against noise on the RFs. It has been recommended
156 in the case of oceanic island studies, such as the Cape Verde islands (Helffrich et al., 2010),
157 the Seychelles islands (Hammond et al., 2013), and the Canary islands (Lodge et al., 2012;
158 Martinez-Arevalo et al., 2013), and in our case we choose it for its capacity to remove
159 anthropic noise.

160 To estimate the Moho depth below the island of Haiti, we use the Extended-Time
161 Multitaper Frequency domain Cross-Correlation Receiver-Function (ETMTRF) technique of

Helffrich (2006), which is based on the MTRF method of Park and Levin (2000). The ETMTRF method uses a series of short and overlapping multiple tapers which window the time series across its full length, and sum the individual Fourier transformed signals to produce a RF estimate.

2.3- Moho depth and Vp/Vs estimation

We use a receiver function stacking technique (H-κ stacking) developed by Zhu and Kanamori (2000) to estimate the Moho depth (H) and the bulk crust ratio V_p/V_s (κ). This method uses the following equations (1), (2), (3), and (4) for stacking the RFs, and gives the results on a 10,000 point grid which shows the plausible range of values for H on increments of 0.4 km between 10 and 50 km and κ on increments of 0.004 between 1.6 and 2.0 (Christensen, 1996):

$$s(H,\kappa)=\sum_{j=1}^{N} w_1 r_j(t_1)+ w_2 r_j(t_2)- w_3 r_j(t_3), \quad (1)$$

$$t_1= H\left[\sqrt{\frac{1}{V_s^2}- p^2}- \sqrt{\frac{1}{V_p^2}- p^2}\right], \quad (2)$$

$$t_2= H\left[\sqrt{\frac{1}{V_s^2}- p^2}+ \sqrt{\frac{1}{V_p^2}- p^2}\right], \quad (3)$$

$$t_3= 2H\sqrt{\frac{1}{V_s^2}- p^2}, \quad (4)$$

where w_1, w_2, w_3 are weights, $r_j(t_i)$ are the amplitudes at the arrival times for each of the raypaths evaluated, N is the number of receiver functions, and p is the ray parameter determined from the IASPEI travel time tables (Kennet, 1991). The weights were

chosen as w_1 = 0.5, w_2 = 0.3 and w_3 = 0.2 as suggested by Zhu and Kanamori (2000). The errors in the results were calculated by taking the maximum axes of the 95% confidence interval of the grid plotted using the Zhu and Kanamori (2000) stacking method. The H-κ stack was performed assuming a mean crustal P-wave velocity (V_p) of 6.6 km/s. This mean crustal P-wave velocity comes from a study of the Pg seismic phase over Hispaniola (McNamara et al., 2012). Crustal thickness, H, and average Vp/Vs determination is not very sensitive to variations in the average Vp, as pointed out by Zhu and Kanamori (2000), and testing Vp within the range 6.4-6.7 km/s on increments of 0.1 km/s provides very similar results of H and Vp/Vs ratio.

Our final analysis uses the RFs computed from 149 earthquakes, from which one or more reverberant Moho phases (PpPs or PpSs + PsPs) were clearly identifiable.

3- Results

Of the 30 stations, 27 yielded receiver functions with coherent P-to-S arrivals. Of these, 19 displayed PpPs and PpSs + PsPs arrivals as well as Ps, enabling H-κ analysis (Table 1). Examples of stacked receiver functions and H-κ plots for stations PIGN, LGNH, and MGOA are shown in Figure 4. For the 8 stations at which no clear reverberant phases were found automatically by the program, RFs were combined to form single station stacks and enhance the signal of the reverberations. At these stations, a clear Ps arrival is identifiable and can be picked manually, but the H-κ stacking technique cannot be performed. We can still however estimate the Moho depth using equation (2) and by assuming a Vp/Vs ratio after several tests. Final Vp/Vs ratios chosen are the values providing arrival times for the PpPs and PpSS + PsPs reverberations that match the signal stacks, and which are coherent

204 with the Vp/Vs of the surrounding stations (Table 2).

205 The results show large but systematic variations in Moho depth and V_p/V_s ratio
206 throughout Haiti (Figures 5 and 6). The Moho depths can be split into three main groups
207 shown in Fig. 5 and based on location and values (in latitudinal order GGIL, MEND, STRA,
208 PIGN and CAYH in the northern part of Haiti; BOIS, DROU, GADC, THOM, CANG, DUFF, MIRB,
209 ARCH, GIMB, BMCA, CBOQ, BMES, PAPH and LGNH in the central part, and MGOA, PETG,
210 GRBO, JAKH, JACM, FERM, FURC, and MARG in the southern part of Haiti).

211

212 **3.1- Moho depths in Haiti**

213 Results from the H-K stacking method in the northern domain of Haiti are well
214 resolved, with the stations STRA, PIGN and CAYH particularly well constrained. Results are
215 also consistent across this domain giving Moho depths of between 20.1 km and 28.2 km
216 (Table 1, Fig. 5).

217 Results in the southern part of Haiti are also well resolved, with the stations MGOA,
218 JACM and PETG particularly well constrained. Results across the domain give Moho depths
219 ranging between 16.1 km and 29.8 km, increasing in the center of the area at the stations
220 GRBO, MARG, FURC (Table 1, Fig. 5). The stations MARG and JAKH have clearly identifiable
221 Ps arrivals, but due to the lack of observable multiples the H-K stacking technique cannot
222 be performed. However, we can still estimate the depth of the Moho by using equation (2)
223 (Table 2, Fig. 5).

224 Our results show that the central part of Haiti exhibits greater Moho depths than in
225 the northern and southern parts, with a Moho discontinuity always deeper than 30 km. The
226 RFs of the stations located in this part of Haiti are more complicated due to intracrustal

reverberations, probably due to sediments layers. However, consistent values are found for the stations THOM, CANG, DUFF, BMCA, CBOQ, DROU, LGNH and BOIS with Moho depths ranging between 34.6 km and 45.2 km (Table 1, Fig. 5). We estimate the Moho depth for the stations GADC, MIRB, GIMB, BMES, ARCH, and PAPH by assuming a Vp/Vs ratio from the closest stations (Table 2, Fig. 5). Transect A in Fig. 7 shows the abrupt change in Moho depth of ~10 km between the southern part and the central part of Haiti.

3.2- Vp/Vs ratio

The average crustal Vp/Vs ratio is sensitive to the bulk composition of the crust (Zandt and Ammon, 1995; Chevrot and Van der Hilst, 2000, Stuart et al., 2006). Mineralogy is an important factor influencing Vp/Vs ratio (Christensen, 1996): For felsic quartz-rich rocks, such as granite, Vp/Vs ratio is ~1.71; for intermediate rocks, such as diorite, Vp/Vs ratio is typically ~1.78; and for mafic rocks, such as gabbro Vp/Vs ratio is ~1.87. Higher values of Vp/Vs ratio are associated with the presence of partial melting or fluids (Watanabe, 1993; Thompson et al., 2010).

The Vp/Vs ratio over Haiti ranges from 1.64 to 1.99 (Fig. 6) suggesting a wide range of mineral composition lateral variation. In particular, the stations MEND, CANG, BMCA and LGNH show particularly high Vp/Vs ratios of 1.94, 1.99, 1.98 and 1.96 respectively (Fig. 6). We observe that these stations are located on or near major tectonic features (Fig. 2), and therefore fluid migration along active faults could feasibly locally increase the Vp/Vs ratio. In order to interpret regional variations in crustal structure and since the interstation variability is relatively high, we calculate the mean Vp/Vs ratio for each of the 3 domains identified in Fig. 5, excluding the four very high values. Regional averages of Vp/Vs seem to

provide more insights than single-station values, excepting for particularly high values that could show fluid migration (Rossi et al., 2006). The mean Vp/Vs ratio is 1.75 ± 0.10 in the northern part of Haiti, 1.80 ± 0.05 in the central part, and 1.80 ± 0.03 in the southern part.

3.3- Shallow discontinuity

In addition to P to S Moho converted phases, one station, CAYH, exhibits another clear shallow discontinuity. The RF plot for station CAYH versus back-azimuth (top of Fig. 8) shows a shallow discontinuity in the first 2 s of the signal, prior to the Ps arrival from the Moho. Clear Moho Ps arrivals are obvious just after 2 s, and are easily identified in the upper RFs (group a, Fig. 8), coming from the south (back-azimuths between 176° and 178°, Fig. 8). The H-K stack method for this group gives a Moho depth of 22.1 km, which is consistent with the closest station PIGN (Fig. 5 and Table 1), and a Vp/Vs ratio of 1.64. We estimate the depth of the shallow discontinuity easily visible in the RFs of the group b assuming that the upper crust has an average Vp of 5.8 km/s and an average Vp/Vs ratio of 1.77. These average properties are derived from the P velocity model in Haiti of Douilly et al. (2013). This discontinuity is thus estimated at ~9.7 km depth.

4- Discussion

4.1- Identification of 3 distinct crustal domains

The depth distribution of the Moho in Haiti shows 3 distinct regions that we relate to 3 distinct geological domains (Fig. 9).

The Southern Peninsula of Hispaniola (Fig. 9) is known to be a part of the Caribbean LIP, and to be composed of Cretaceous tholeitic material (Calmus, 1983; Bien-Aimé

Momplaisir, 1986). In this part of the island, the Moho depths from our study vary from 16.1 km to 29.8 km along a W-E profile (Fig. 7E) and from 20.5 km to 27.5 km along a N-S profile (Fig. 7A), giving an average crustal thickness of 22 ± 5 km. The variability of the Moho depths we image in the Southern Peninsula may reflect the large differences in the LIP thickness identified in previous studies between the oceanic crust and the areas with more or less of underplated material (Diebold et al., 1981; Mauffret and Leroy, 1997; Leroy et al., 2000; Mauffret et al., 2001). In our results the mean Vp/Vs ratio is 1.80 ± 0.03, consistent with previous studies (Douilly et al., 2013) and the geology of the Southern Peninsula (Calmus, 1983; Bien-Aimé Momplaisir, 1986). The northern limit of the LIP crustal domain is given by the Moho depth calculated at the station LGNH (34.6 km; Fig. 5) and could correspond to the trace of the EPGFZ (Fig. 2) in this area (south of LGNH), as suggested by previous studies (Saint-Fleur et al., 2015).

The northern part of Hispaniola (Fig 9) is known to be a part of the Great Arc of the Caribbean (Burke, 1988), an inactive intra-oceanic island arc formed in the Cretaceous at the boundary of the Pacific domain and the proto-Caribbean oceanic crust (Pindell et al., 2006). The Moho depth values we compute are ranging between 20.1 km and 28.2 km, providing an average crustal thickness of 23 ± 3 km in agreement with the values found in southern Cuba (approximately 20 km, Moreno et al., 2002; Gonzalez et al., 2012) and eastern Hispaniola (about 24 km, Nuñez et al., 2015). Furthermore, our results delineate the southwestern limit of the island arc domain. The shift of the Moho depths, from 22.1 km (CAYH) to 36.4 km (GADC), occurs across the trace of a major thrust evidenced by geological studies (Figs 5 and 9). Both this major thrust and the sharp offset of the Moho depths outline a distinct crustal domain to the west and south of this feature.

In addition to the southern and northern domains discussed above, we identify a central domain distinct from both the LIP in the South and the island arc in the North (Fig. 9), which is characterized by a thicker crust ranging from 32.3 km to 45.4 km, with an average of 41 ± 4 km. The relatively deep Moho is well constrained by 13 stations. In addition, the preliminary results of a recent seismic refraction study by Nuñez et al. (2015) indicate that the thickness of the crust increases from eastern Hispaniola towards the west reaching a value of ~40 km at the boundary between Haiti and the Dominican Republic near our profile. The Cul-de-Sac sedimentary basin (Fig. 1) and the Trans-Haitian belt belong to the same thick domain, where the nature of the crust below these superficial structures has still to be determined. We further discuss the different hypothesis regarding the nature of the crust of this domain.

4.2 Vp/Vs ratio

We find very high Vp/Vs ratios, between 1.94 and 1.99 at four stations, located near major faults: LGNH near the strike-slip EPGFZ and MEND, CANG and BMCA near the main thrust faults (Figs. 2 and 6). High Vp/Vs ratios are often associated with partial melt, basaltic intrusions or the presence of fluids (Stuart et al, 2006; Hammond et al., 2011). We favor an explanation whereby the high Vp/Vs ratios associated with major crustal faults are related to the presence of fluids within the fault zones (Thurber et al., 2003; Zhao et al., 1996). Nevertheless, all the stations located near major faults do not present high Vp/Vs values (e.g. CAYH, fig. 2).

The mean Vp/Vs ratio (1.80 ± 0.03) found in the southern domain is in agreement with its late Cretaceous oceanic plateau origin (Christensen, 1996; Douilly et al., 2013). In

319 the northern domain composed of a late Cretaceous–Eocene, intra–oceanic volcanic arc
320 and forearc–accretionary prism, the Vp/Vs ratio of 1.75 ± 0.10 is close to that expected
321 for the average continental crust, 1.768 (Christensen, 1996). The central part of Haiti is
322 characterized by Vp/Vs ratio of 1.80 ± 0.05, indicating that mafic rocks may be part of the
323 crustal lithology of this domain as in the southern domain.
324
325 **4.3- Implications for the tectonic history of Hispaniola**
326 We identify three distinct tectonic domains with different crustal thickness and bulk
327 composition. Based on our computed Moho depths and Vp/Vs ratios, and with additional
328 constraints from the major thrusts identified at the surface and the geodynamic
329 reconstructions (Leroy et al., 2000; Pubellier et al., 2000; Calais et al., 2016), we propose a
330 geological model along a N-S profile across Haiti (Fig. 10). This transect shows the LIP in the
331 South, the Cretaceous volcanic arc in the North, and a central thicker domain.
332 The central domain is characterized by relatively thick crust of ~41 km, between two
333 domains with significantly thinner crusts of 20-30 km. Surprisingly, the thick crust of the
334 central domain is not associated with major relief (~1 km). Based on field studies and
335 geodynamic reconstructions proposed for this area (e.g. Stéphan et al., 1990; Meschede and
336 Frisch,1998; Mann et al 1991; Calais et al., 2016), the nature of the crust of the central
337 domain is likely to be island arc and fore-arc type, considered as either back-arc (Mann and
338 Lawrence, 1991) or a Cretaceous-Eocene remnant arc (Heubeck et al., 1991). Other
339 stratigraphic and tectonic studies (e.g. Pubellier et al., 2000) suggest that the fold-and-
340 thrust belt of this crustal domain may be rooted on the continuation of the rifted crust of
341 the eastern Cayman continental passive margin (Fig. 9). However, Vp/Vs ratio of 1.80,

typical for mafic rocks (average of values for this domain; Tables 1 & 2), may indicate that the central crustal domain could not be composed only of island arc crust, and may imply the presence of dense material. This dense material could be either related to Pliocene-Quaternary mafic center of volcanism coming from an ancient continental mantle lithosphere fragment (Kamenov et al., 2011) or associated to LIP material fragment coming from the south and both trapped early in central Haiti. Geochemical studies of the LIP south of Hispaniola from submersible dive samples (Revillon et al., 2000; Mauffret et al., 2001) show indeed that the lower part of the LIP is made of ultra-mafic rocks and geophysical studies (Mauffret and Leroy, 1997; 1999) evidence a high velocity layer composed of dense material (velocity 7.5 to 7.9 km/s; density of 3 to 3.1; Herzberg et al., 1983). The mafic Quaternary rocks are also MgO-rich (Kamenov et al 2011) and give high Vp/Vs ratio.

On the transect in Fig. 10 we also draw the intracrustal discontinuity determined from our receiver functions at the station CAYH. The estimated depth of this intracrustal discontinuity (~10 km) may provide information on the possible depth for the Late-Cretaceous to Pleistocene flysch of the Peralta belt (Witschard and Dolan, 1990; Dolan et al., 1991), which outcrops at the front of the Cretaceous volcanic arc (Fig. 10). At the surface, three major thrusts are geologically mapped (the Montagnes Noires, the Chaîne des Matheux and the Gonâve Island; Fig. 1 and 2; Mann et al., 1995; Pubellier et al., 2000; Hernaiz Huerta et al., 2007). In our transect, we propose to extend these thrusts to greater depth along three large crustal slices (Fig. 10). The three major thrusts of the Trans-Haitian belt show small cumulative throws at outcrop and little evidence of strong compressional tectonics (Mann et al 1995; Pubellier et al 2000, Corbeau et al., 2016b). SW-vergent fold

and thrust belt related to the Hispaniola restraining bend and back arc basin collapse (Heubeck et al., 1991) could have contributed to the overall thickening.

5- Conclusions

A receiver function study of 23 stations is used to determine the crustal structure across Haiti, in order to place better constraints on the history and geometry of late Cretaceous to recent terrane accretion. In the northern part of Haiti, consisting of the Cretaceous volcanic island arc and forearc of the Greater Antilles, the Moho discontinuity is imaged at a depth of ~23 km with Vp/Vs ratio of 1.75. In the southern part of Haiti, made of the folded and thrusted Cretaceous oceanic Large Igneous Province (LIP), the Moho depth is imaged at ~22 km, and Vp/Vs ratio is 1.80. In the central part of Haiti, encompassing the Haitian fold-and-thrust belt, the Moho discontinuity is deeper with a mean depth of ~41 km. We propose that this unexpected thick central domain with Vp/Vs ratio of 1.80 corresponds to a distinct crustal domain. This domain is likely to consist of island-arc type crust related to the Great Arc of the Caribbean, or the proximal part of the Cayman Trough eastern passive margin, associated with mafic material coming from fragments of lithospheric mantle from the north or mafic LIP material from the south.

Acknowledgements

The seismological equipment was loaned from the SEIS-UK equipment pool and from the ISTeP facilities. The facilities of SEIS-UK are supported by the Natural Environment

Research Council (NERC) under Agreement R8/H10/64. DK time on the research is funded by NERC grant NE/L013932/1. This work could not have been done without Gérard Laborde and DIGICEL, and without our collaboration with the Bureau des Mines et de l'Energie and the Université d'Etat d'Haiti in Haiti. The paper benefits from fruitful discussions with Nicolas Bellahsen and Claudio Rosenberg. We thank the Editor, the reviewer David Schlaphorst and an anonymous reviewer for their constructive comments that helped improved the manuscript.

References

Abers, G. A., X. Hu and L. R. Sykes, 1995. Source scaling of earthquakes in the Shumagin region, Alaska : time-domain inversions of regional waveforms. *Geophysical Journal International,* vol. 123, no 1, p. 41–58.

Ammon, C. J., 1991. The isolation of receiver effects from teleseismic P waveforms. *Bull. Seismol. Soc. Am,* vol. 81, no 6, p. 2504–2510.

Bien-Aimé Momplaisir, R., 1986. Contribution à l'étude géologique de la partie orientale du Massif de la Hotte (Presqu'île du Sud d'Haïti) : Synthèse structurale des marges de la presqu'île à partir de données sismiques, thèse de doctorat, Ph. D. thesis, 210 pp., Univ. Pierre-et-Marie-Curie (Paris VI), Paris.

Boisson, D., 1987. Etude geologique du massif du nord d'Haiti (Hispaniola-grandes Antilles), thèse de doctorat, Ph. D. thesis, Univ. Pierre et Marie Curie (Paris VI), Paris.

Bowin, C.O, 1976. Caribbean Gravity Field and Plate Tectonics, Geological Society of America Special Paper, vol. 169.

Burke, K.,1988. Tectonic evolution of the Caribbean, Annual Review of Earth and Planetary Sciences, vol. 16, p. 201-230.

Calais, E. and B. Mercier de Lepinay, 1991. From transtension to transpression along the northern Caribbean plate boundary off Cuba : Implications for the recent motion of the Caribbean plate, *Tectonophysics*, vol. 186, no 3, p. 329–350.

Calais, E., S. Symithe, B. Mercier de Lépinay and C. Prépetit, 2016. Plate boundary segmentation in the northeastern Caribbean from geodetic measurements and Neogene geological observations, *Comptes Rendus Geoscience*, *348*(1), 42-51.

Calmus, T., 1983. Contribution à l'étude géologique du massif de Macaya(sud-ouest d'Haïti, Grandes Antilles) : sa place dans l'évolution de l'orogène Nord-Caraïbe, thèse de doctorat, Univ. Paris VI, Paris.

Chevrot, S. and R. D. van der Hilst, 2000. The poisson ratio of the australian crust : geological and geophysical implications, *Earth and Planetary Science Letters*, vol. 183, no 1, p. 121–132.

Christensen, N. I., 1996. Poisson's ratio and crustal seismology, *Journal of Geophysical Research*: Solid Earth (1978–2012), vol. 101, no B2, p. 3139–3156.

Corbeau, J., F. Rolandone, S. Leroy, B. Mercier de Lépinay, B. Meyer, N. Ellouz-Zimmermann and R. Momplaisir, 2016a. The Northern Caribbean plate boundary in the Jamaica Passage: structure and seismic stratigraphy, *Tectonophysics*, doi:10.1016/j.tecto.2016.03.022.

Corbeau, J., F. Rolandone, S. Leroy, B. Meyer, B. Mercier de Lépinay, N. Ellouz-Zimmermann and R. Momplaisir, 2016b. How transpressive is the Northern Caribbean plate boundary ?, *Tectonics,* doi:10.1002/2015TC003996.

Cruz-Orosa, I., F. Sàbat, E. Ramos, L. Rivero and Y. M. Vázquez-Taset, 2012. Structural evolution of the La Trocha fault zone : Oblique collision and strike-slip basins in the Cuban Orogen, *Tectonics*, vol. 31, no 5.

Diebold, J., P. Stoffa, P. Buhl and M. Truchan, 1981. Venezuela Basin crustal structure, *Journal of Geophysical Research* : Solid Earth (1978–2012), vol. 86, no B9, p. 7901–7923.

Dolan, J., P. Mann, R. de Zoeten, C. Heubeck, J. Shiroma and S. Monechi, 1991. Sedimentologic, stratigraphic, and tectonic synthesis of Eocene-Miocene sedimentary basins, Hispaniola and Puerto Rico, *Geological Society of America Special Papers*, vol. 262, p.217–264.

Douilly, R., J. S. Haase, W. L. Ellsworth, M.-P. Bouin, E. Calais, S. J. Symithe, J. G. Armbruster, B. Mercier de Lépinay, A. Deschamps, S.-L. Mildor and collab., 2013. Crustal Structure and Fault Geometry of the 2010 Haiti Earthquake from Temporary Seismometer Deployments, Bulletin of the Seismological Society of America, vol. 103, no 4, p. 2305–2325.

Duncan, R. and R. Hargraves, 1984. Plate tectonic evolution of the Caribbean region in the mantle reference frame, *Geological Society of America Memoirs*, vol. 162, p. 81–94.

Escuder Viruete, J., Contreras F., Stein, G., Urien, P., Joubert, M., Ullrich, T.D., Mortensen, J., Perez Estaun, A., 2006. Transpression and strike-slip partitioning in the Caribbean island arc: fabric development, kinematics and Ar-Ar ages of syntectonic emplacement of the Loma de Cabrera batholith, Dominican Republic, Journal of Structural Geology, 28, 1496-1519.

González, O., B. Moreno, F. Romanelli and G. F. Panza, 2012. Lithospheric structure below seismic stations in Cuba from the joint inversion of Rayleigh surface waves dispersion and receiver functions, *Geophysical Journal International*, vol. 189, p. 1047–1059.

Granja-Bruña, J., A. Carbó-Gorosabel, P. L. Estrada, A. Muñoz-Martín, U. ten Brink, M. G. Ballesteros, M. Druet and A. Pazos, 2014. Morphostructure at the junction between the Beata ridge and the Greater Antilles island arc (offshore Hispaniola southern slope), *Tectonophysics*, vol. 618, p. 138–163.

Gurrola, H., G. E. Baker and J. B. Minster, 1995. Simultaneous time-domain deconvolution with application to the computation of receiver functions, *Geophysical Journal International*, vol. 120, no 3, p. 537–543.

Hammond, J., J.-M. Kendall, G. Stuart, D. Keir, C. Ebinger, A. Ayele and M. Belachew, 2011. The nature of the crust beneath the Afar triple junction : Evidence from receiver functions, *Geochemistry, Geophysics, Geosystems*, vol. 12, no 12.

Hammond, J., J.-M. Kendall, G. Stuart, C. Ebinger, I. Bastow, D. Keir, A. Ayele, M. Belachew, B. Goitom, G. Ogubazghi and collab., 2013. Mantle upwelling and initiation of rift segmentation beneath the Afar Depression, *Geology*, vol. 41, no 6, p. 635–638.

Hastie, A. R., S. F. Mitchell, P. J. Treloar, A. C. Kerr, I. Neill and D. N. Barfod, 2013. Geochemical components in a Cretaceous island arc : The Th/La-(Ce/Ce*)Nd diagram and implications for subduction initiation in the inter-American region, *Lithos*, vol. 162, p. 57–69.

Helffrich, G., 2006. Extended-time multitaper frequency domain cross-correlation receiver-function estimation, *Bulletin of the Seismological Society of America*, vol. 96, no 1, p. 344–347.

Helffrich, G., B. Faria, J. F. Fonseca, A. Lodge and S. Kaneshima, 2010. Transition zone structure under a stationary hot spot: Cape Verde, *Earth and Planetary Science Letters*, vol. 289, no 1, p. 156–161.

Hernaiz Huerta, P.P., Diaz de Neira, J.A., Garcia Senz, J. Deschamps, I., Genna, A., Nicole, N., Lopera, E., Escuder Virruete, J., Ardevol Oro, Ll., Perez Estaun, A., 2007. La estructura del suroeste de la Republica Dominicana: un ejemplo de deformacion en regimen transpresivo, Boletin Geologico y Minero, 118(2) : 337-358.

Herzberg, C., W. Fyfe and M. Carr, 1983. Density constraints on the formation of the continental Moho and crust, *Contributions to Mineralogy and Petrology*, vol. 84, no 1, p. 1–5.

Heubeck, C., P. Mann, J. Dolan and S. Monechi, 1991. Diachronous uplift and recycling of sedimentary basins during cenozoic tectonic transpression, northeastern caribbean plate margin, *Sedimentary geology*, vol. 70, no 1, p. 1–32.

Iturralde-Vinent, M. A., 2006. Meso-Cenozoic Caribbean paleogeography : implications for the historical biogeography of the region, *International Geology Review*, vol. 48, no 9, p. 791–827.

Kamenov, G. D. et al., 2011. Ancient lithospheric source for Quaternary lavas in Hispaniola. *Nature Geoscience*, vol. 4, p. 554–557.

Kennet, B., 1991. IASPEI 1991 seismological tables, *Terra Nova*, vol. 3, no 2, p. 122–122.

Langston, C. A., 1979. Structure under Mount Rainier, Washington, inferred from teleseismic body waves, *Journal of Geophysical Research* : Solid Earth (1978–2012), vol. 84, no B9, p. 4749–4762.

Leroy, S., B. Mercier de Lépinay, A. Mauffret and M. Pubellier, 1996. Structural and tectonic evolution of the eastern Cayman Trough (Caribbean Sea) from seismic reflection data, *AAPG bulletin*, vol. 80, no 2, p. 222–247.

Leroy, S., A. Mauffret, P. Patriat and B. Mercier de Lépinay, 2000. An alternative interpretation of the Cayman trough evolution from a reidentification of magnetic anomalies, *Geophysical Journal International*, vol. 141, no 3, p. 539–557.

Leroy, S., N. Ellouz-Zimmermann, J. Corbeau, F. Rolandone, B. Mercier de Lépinay, B. Meyer, R. Momplaisir, J. L. Granja Bruna, A. Battani, C. Baurion, E. Burov and collab., 2015. Segmentation and kinematics of the North America-Caribbean plate boundary offshore Hispaniola, *Terra Nova*.

Ligorría, J. P. and C. J. Ammon, 1999. Iterative deconvolution and receiver-function estimation, *Bulletin of the seismological Society of America*, vol. 89, no 5, p. 1395–1400.

Lodge, A., S. Nippress, A. Rietbrock, A. García-Yeguas and J. Ibáñez, 2012. Evidence for magmatic underplating and partial melt beneath the canary islands derived using teleseismic receiver functions, *Physics of the Earth and Planetary Interiors*, vol. 212, p. 44–54.

Mauffret, A. and S. Leroy, 1997. Seismic stratigraphy and structure of the Caribbean igneous province, *Tectonophysics*, vol. 283, no 1, p. 61–104.

Mauffret, A., Leroy, S., 1999. Neogene intraplate deformation of the Caribbean plate at the Beata Ridge. Sedimentary Basins of the World 4, 627–669.

Mauffret, A., S. Leroy, É. d'Acremont, A. Maillard, B. Mercier de Lépinay, A. T. Dos Reis, N. Miller, A. Nercessian, R. Pérez-Vega and D. Perez, 2001. Une coupe de la province volcanique Caraïbe : premiers résultats de la campagne sismique Casis 2, *Comptes Rendus de l'Académie des Sciences*-Series IIA-Earth and Planetary Science, vol. 333, no 10, p. 659–667.

Mann, P., G. Draper and J. F. Lewis, 1991. An overview of the geologic and tectonic development of Hispaniola, *Geological Society of America Special Papers*, vol. 262, p. 1–28.

Mann, P. and S. Lawrence, 1991. Petroleum potential of southern Hispaniola, *Journal of Petroleum Geology*, vol. 14, no 2, p. 291–308.

Mann, P., F. Taylor, R. L. Edwards and T.-L. Ku, 1995. Actively evolving microplate formation by oblique collision and sideways motion along strike-slip faults : An example from the northeastern Caribbean plate margin, *Tectonophysics*, vol. 246, no 1, p. 1–69.

Martinez-Arevalo, C., F. de Lis Mancilla, G. Helffrich and A. Garcia, 2013. Seismic evidence of a regional sublithospheric low velocity layer beneath the Canary islands, *Tectonophysics*,

vol. 608, p. 586–599.

McNamara, D., M. Meremonte, J. Maharrey, S.-L. Mildore, J. Altidore, D. Anglade, S. Hough, D. Given, H. Benz, L. Gee and collab., 2012. Frequency-dependent seismic attenuation within the Hispaniola Island region of the Caribbean Sea, *Bulletin of the Seismological Society of America*, vol. 102, no 2, p. 773–782.

Meschede, M. and W. Frisch, 1998. A plate-tectonic model for the Mesozoic and Early Cenozoic history of the Caribbean plate, *Tectonophysics*, vol. 296, no 3, p. 269–291.

Moreno, B., M. Grandison and K. Atakan, 2002. Crustal velocity model along the southern Cuban margin : implications for the tectonic regime at an active plate boundary, *Geophysical Journal International*, vol. 151, no 2, p. 632–645.

Nuñez, D., D. Cordoba, F. J. Nuñez-Cornu and M. O. Cotilla, 2015. Lithosphere structure from Cordillera Central to Cordillera Oriental (Dominican Republic), *EGU General Assembly Conference Abstracts*, vol. 17, p. 14467.

Owens, T., S. Taylor and G. Zandt, 1983. Isolation and enhancement of the response of local seismic structure from teleseismic P-waveforms, *cahier de recherche*, Lawrence Livermore National Lab., CA (USA).

Park, J. and V. Levin, 2000. Receiver functions from multiple-taper spectral correlation estimates, *Bulletin of the Seismological Society of America*, vol. 90, no 6, p. 1507–1520.

Pindell, J., L. Kennan, K. P. Stanek, W. Maresch and G. Draper, 2006. Foundations of Gulf of Mexico and Caribbean evolution: eight controversies resolved, *Geologica Acta*, vol. 4, no 1-2, p. 303.

Pindell, J., W. V. Maresch, U. Martens and K. Stanek, 2012. The Greater Antillean Arc : Early Cretaceous origin and proposed relationship to Central American subduction mélanges : implications for models of Caribbean evolution, *International Geology Review*, vol. 54, no 2, p. 131–143.

Pubellier, M., A. Mauffret, S. Leroy, J. M. Vila and H. Amilcar. 2000, «Plate boundary readjustment in oblique convergence : Example of the Neogene of Hispaniola, Greater Antilles», Tectonics, vol. 19, no 4, p. 630–648.

Revillon, S., E. Hallot, N. Arndt, C. Chauvel and R. Duncan, 2000. A complex history for the Caribbean Plateau: petrology, geochemistry, and geochronology of the Beata Ridge, South Hispaniola, *The Journal of Geology*, vol. 108, no 6, p. 641–661.

Rossi, G., Abers, G. A., Rondenay, S., & Christensen, D. H., 2006. Unusual mantle Poisson's ratio, subduction, and crustal structure in central Alaska, *Journal of Geophysical Research: Solid Earth*, vol. 111, no B9.

Saint Fleur, N., N. Feuillet, R. Grandin, E. Jacques, J. Weil-Accardo and Y. Klinger, 2015. Seismotectonics of southern Haiti: A new faulting model for the 12 january 2010 M7 earthquake, *Geophysical Research Letters*.

Symithe, S. and E. Calais, 2016. Present-day shortening in Southern Haiti from GPS measurements and implications for seismic hazard, *Tectonophysics*, *679*, 117-124.

Symithe, S., E. Calais, J. B. Chabalier, R. Robertson and M. Higgins, 2015. Current block motions and strain accumulation on active faults in the Caribbean, *Journal of Geophysical Research: Solid Earth*, *120*(5), 3748-3774.

Stéphan, J.-F., B. Mercier de Lépinay, E. Calais and M. Tardy, 1990. Paleogeodynamic maps of the Caribbean: 14 steps from Lias to Present, *Bull. Soc. géol.* Ft, p. 0–6.

Stuart, G., I. Bastow and C. Ebinger, 2006. Crustal structure of the northern Main Ethiopian Rift from receiver function studies, *Geological Society*, London, Special Publications, vol. 259, no 1, p. 253–267.

Thompson, D., I. Bastow, G. Helffrich, J. Kendall, J. Wookey, D. Snyder, and D. Eaton, 2010. Precambrian crustal evolution: Seismic constraints from the Canadian Shield, *Earth Planet. Sci. Lett.*, 297, 655–666, doi:10.1016/j.epsl.2010.07.021.

Thurber, C., S. Roecker, K. Roberts, M. Gold, L. Powell and K. Rittger, 2003. Earthquake locations and three-dimensional fault zone structure along the creeping section of the San Andreas fault near Parkfield, CA : Preparing for SAFOD, *Geophysical Research Letters*, vol. 30, no 3.

VanDerLelij, R., 2013. Reconstructing north-western Gondwana with implications for the evolution of the Iapetus and Rheic Oceans: a geochronological, thermochronological and geochemical study, thèse de doctorat, University of Geneva.

Watanabe, T., 1993. Effects of water and melt on seismic velocities and their application to characterization of seismic reflectors, *Geophysical Research Letters*, vol. 20, no 24, p. 2933–2936.

Witschard, M. and J. F. Dolan, 1990. Contrasting structural styles in siliciclastic and carbonate rocks of an offscraped sequence: The Peralta accretionary prism, Hispaniola, *Geological Society of America Bulletin*, vol. 102, no 6, p. 792–806.

Zandt, G. and C. J. Ammon, 1995. Continental crust composition constrained by measurements of crustal Poisson's ratio, *Nature*, vol. 374, no 6518, p. 152–154.

668 Zhao, D., H. Kanamori, H. Negishi and D. Wiens, 1996. Tomography of the source area of
669 the 1995 kobe earthquake : evidence for fluids at the hypocenter ?, *Science*, vol. 274, no
670 5294, p. 1891–1894.
671 Zhu, L. and H. Kanamori, 2000. Moho depth variation in southern California from
672 teleseismic receiver functions, *Journal of Geophysical Research* B, vol. 105, no B2, p. 2969–
673 2980.

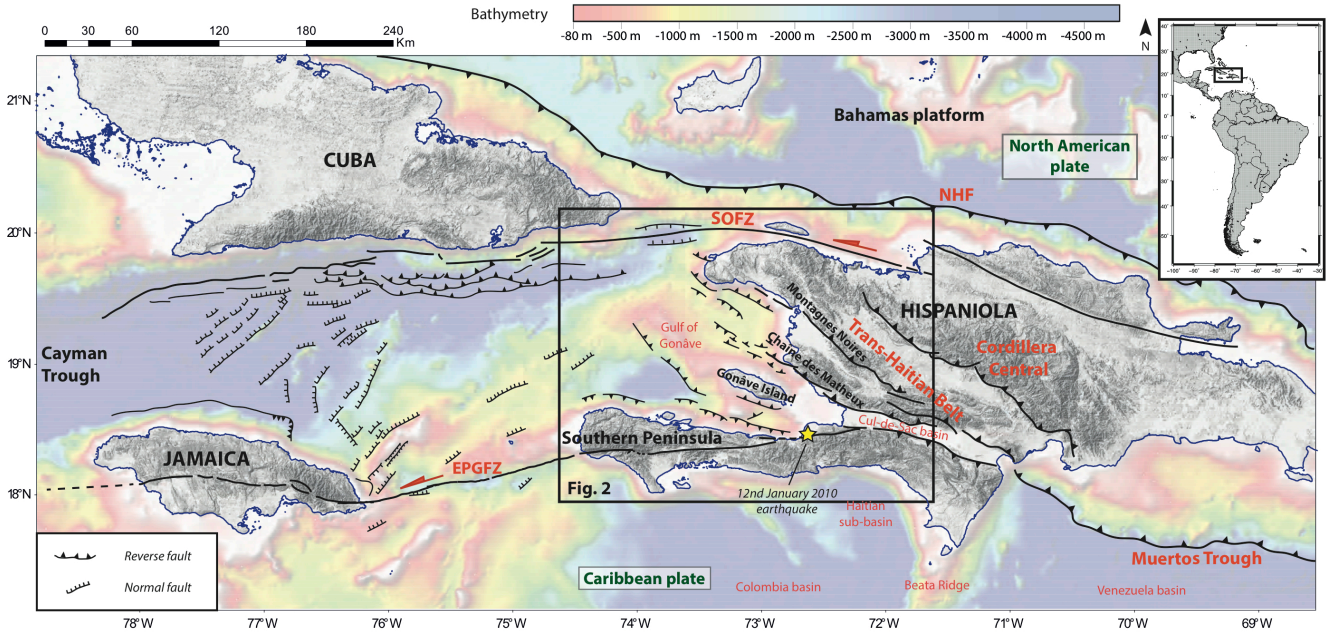

Figure 1: Tectonic map of the Northern Caribbean plate boundary. Faults are from previous studies (Calais and Mercier de Lépinay, 1991; Mann et al., 1995; Leroy et al., 1996; 2015; Granja Bruna et al., 2014). NHF: North-Hispaniola Fault; SOFZ: Septentrional-Oriente Fault Zone; EPGFZ: Enriquillo-Plantain-Garden Fault Zone.

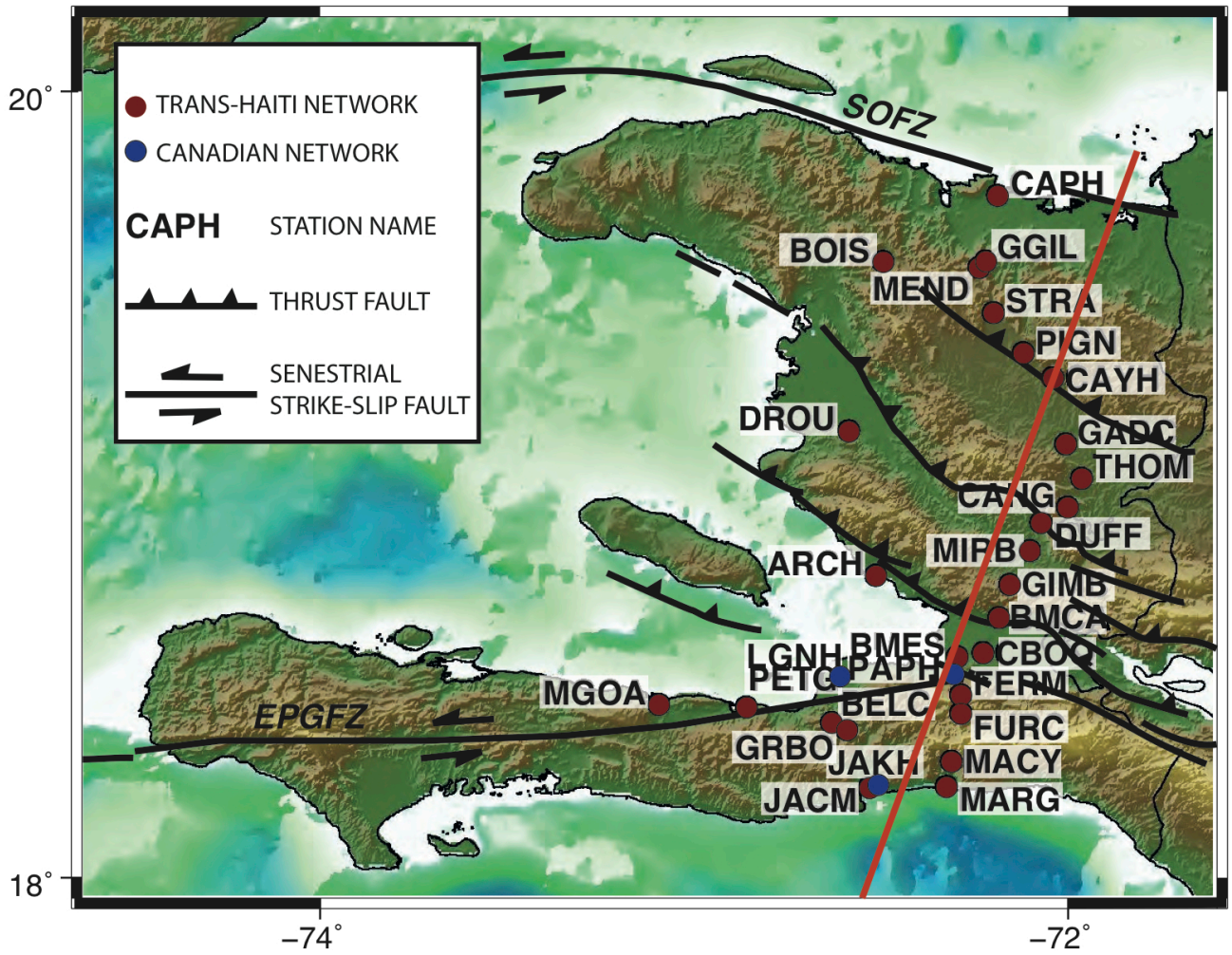

Figure 2: Locations of the seismic stations used in this receiver function study in Haiti, superimposed on the topographic map and with the major tectonic features. Red circles are the stations of the Trans-Haiti network and blue circles are the 3 permanent stations of the Canadian National Network. Faults are from Pubellier et al. (2000). SOFZ: Septentrional-Oriente Fault Zone; EPGFZ: Enriquillo-Plantain-Garden Fault Zone. The red line indicates the localization of the transect proposed Fig. 10.

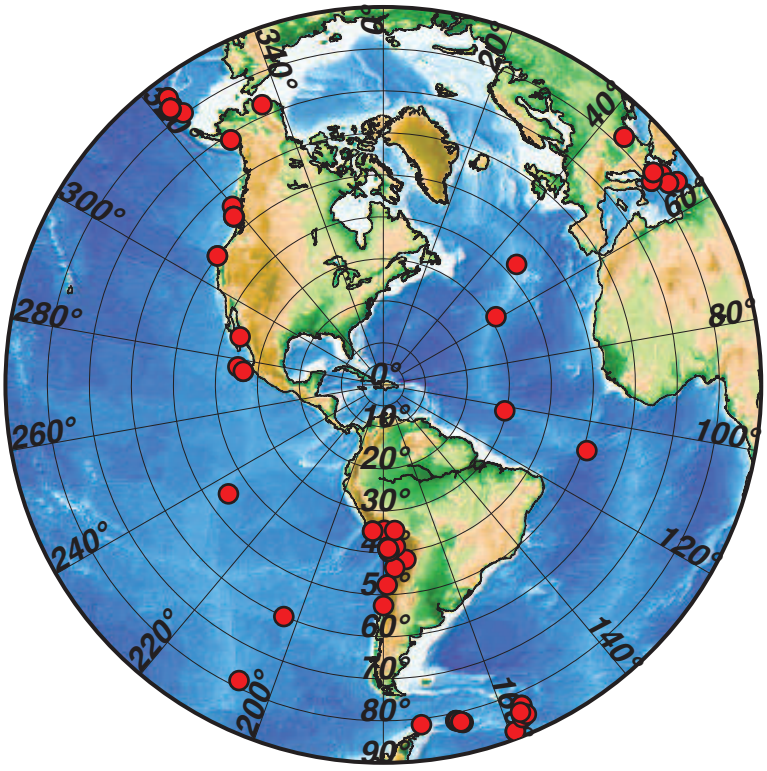

688

689 **Figure 3:** Global distribution of the earthquakes used when computing Receiver Functions.

690 They are plotted with an azimuthal equidistant map projection around our network.

691

i.

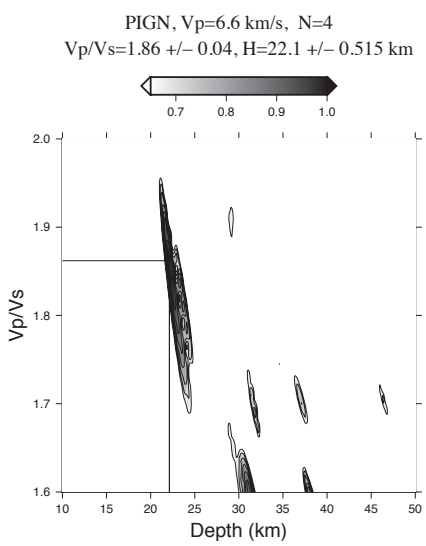
PIGN, Vp=6.6 km/s, N=4
Vp/Vs=1.86 +/– 0.04, H=22.1 +/– 0.515 km
0.7 0.8 0.9 1.0
Vp/Vs
Depth (km)

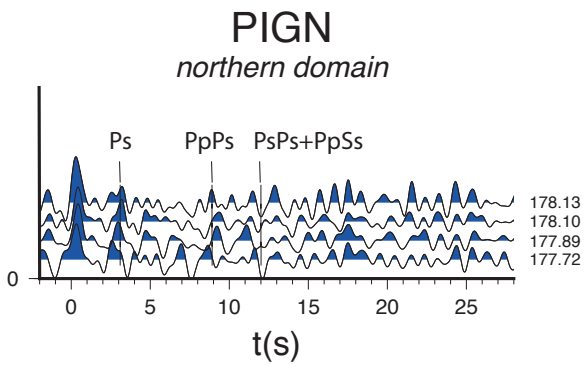
PIGN
northern domain
Ps
PpPs
PsPs+PpSs
178.13
178.10
177.89
177.72
0
t(s)

ii.

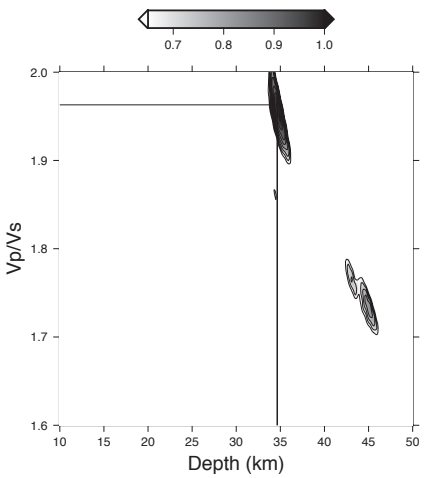
LGNH, Vp=6.6 km/s, N=8
Vp/Vs=1.96 +/– 0.021, H=34.6 +/– 0.435 km
0.7 0.8 0.9 1.0
Vp/Vs
Depth (km)

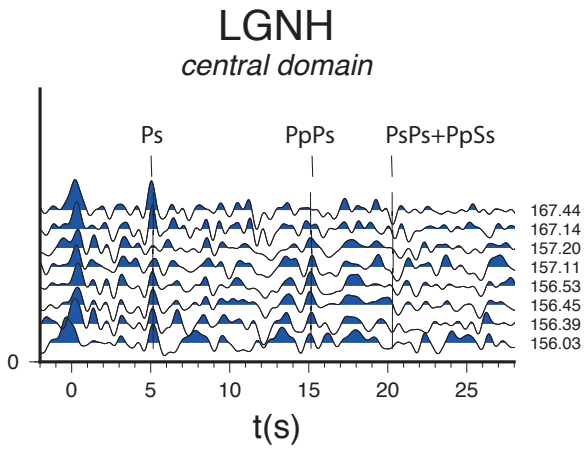
LGNH
central domain
Ps
PpPs
PsPs+PpSs
167.44
167.14
157.20
157.11
156.53
156.45
156.39
156.03
0
t(s)

iii.

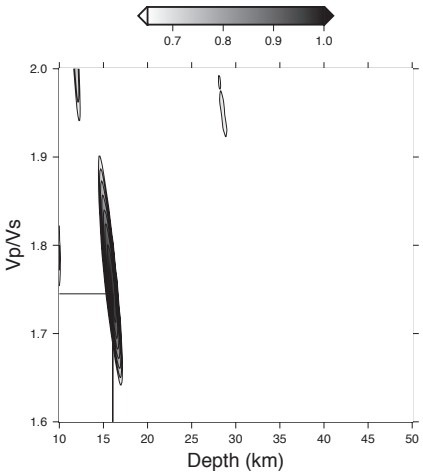
MGOA, Vp=6.6 km/s, N=10
Vp/Vs=1.74 +/– 0.044, H=16.1 +/– 0.485 km
0.7 0.8 0.9 1.0
Vp/Vs
Depth (km)

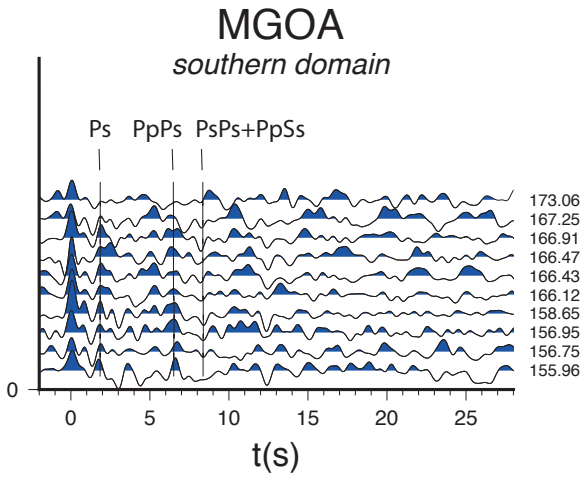
MGOA
southern domain
Ps
PpPs
PsPs+PpSs
173.06
167.25
166.91
166.47
166.43
166.12
158.65
156.95
156.75
155.96
0
t(s)

Figure 4: Examples of Moho depth (H) versus Vp/Vs plots (left) from the method of Zhu and Kanamori (2000) and receiver functions associated (right) for one station of each domain. On each receiver function the arrival time of the Moho phase Ps (t1) and the reverberations PpPs (t2) and PsPs+PpSs (t3) are marked based on the results of the H-K stack (Table 1) and the equations (2) to (4). The receiver functions are plotted as a function of the back-azimuth (number at the right of each trace). See Figs. 2 and 5 for the location of the stations and the different domains.

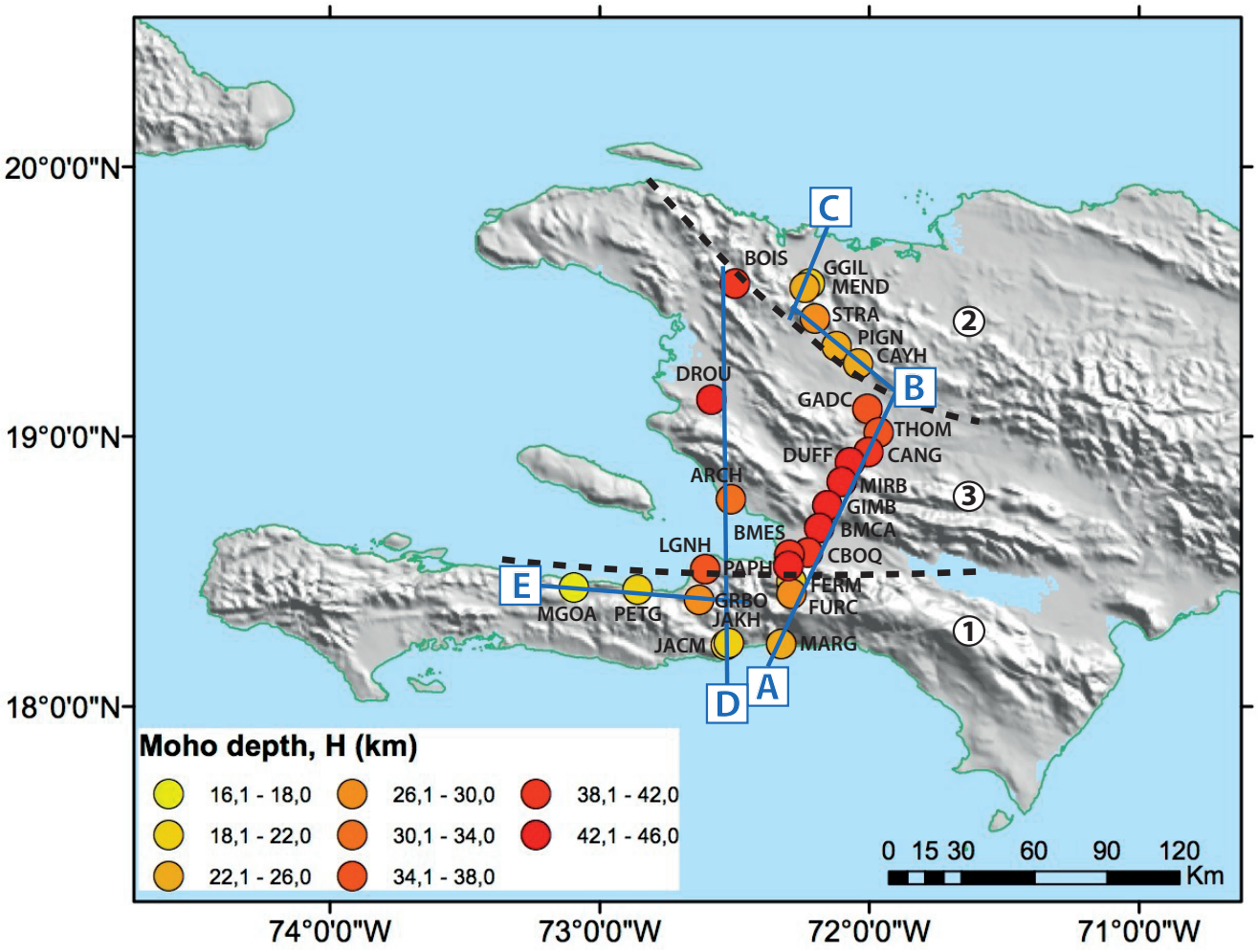

Figure 5: Variations in Moho depth (Tables 1 and 2) across Haiti determined from receiver function analysis. The blue lines A, B, C, D, and E show the orientation of transects in Figure 7. The black dashed lines delimit the boundary between 3 distinct domains of Moho depth values, numbered 1, 2 and 3 (see text for explanation).

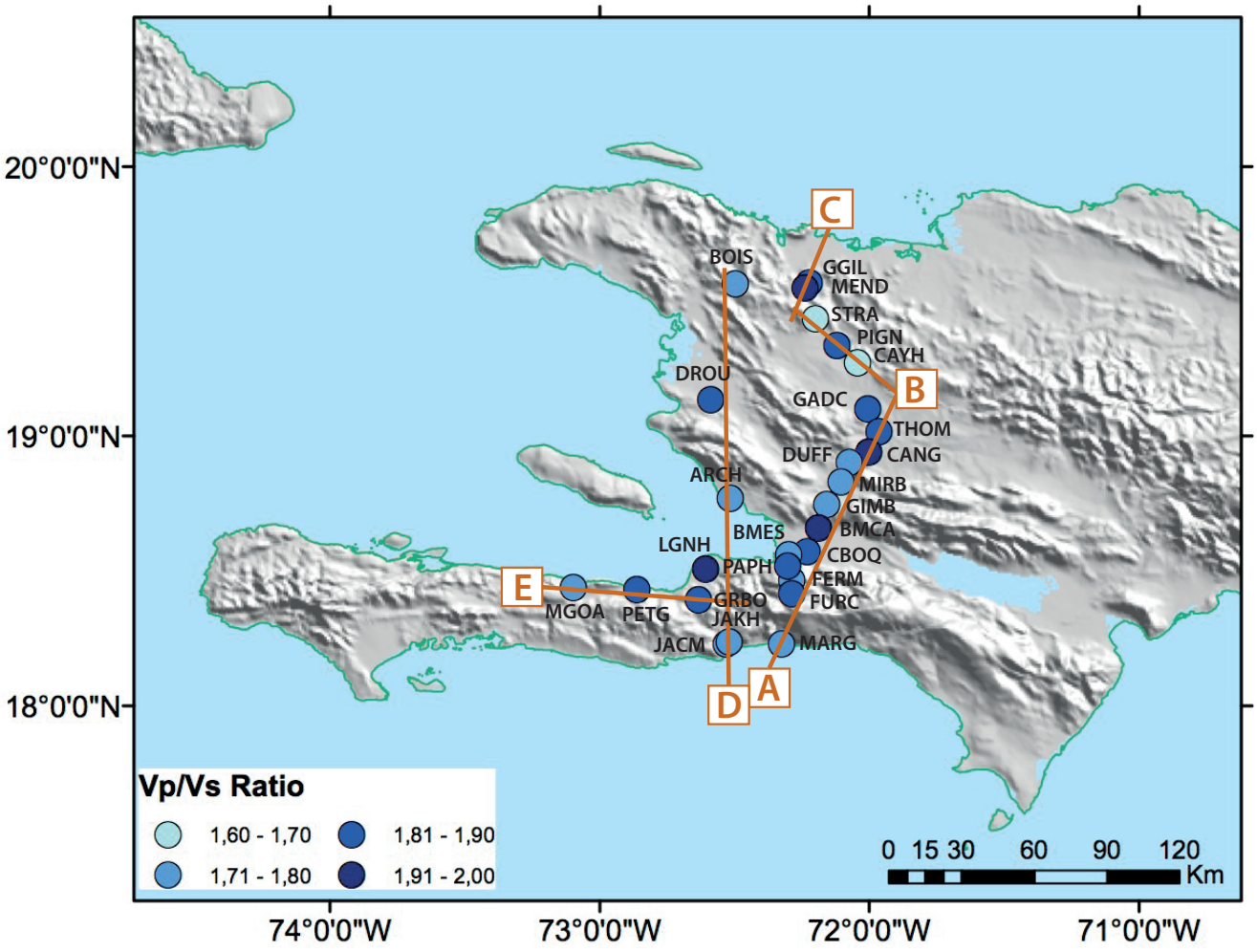

Figure 6: Variations in Vp/Vs ratio (Tables 1 and 2) across Haiti determined from receiver function analysis. The orange lines A, B, C, D, and E show the orientation of transects in Figure 7.

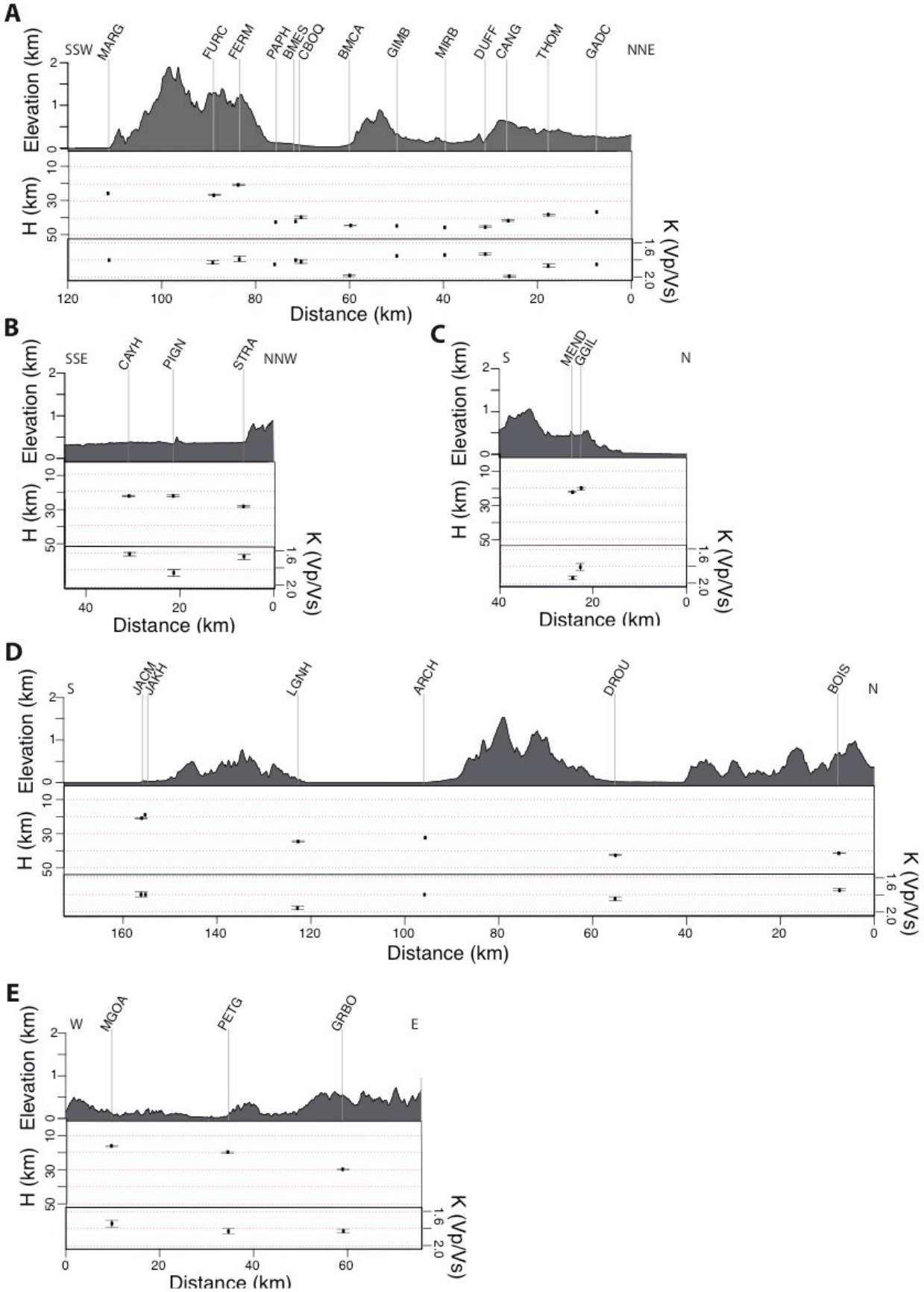
A
SSW
MARG
FURC
FERM
PAPH
BMES
CBOO
BMCA
GIMB
MIRB
DUFF
CANG
THOM
GADC
NNE
Elevation (km)
H (km)
K (Vp/Vs)
Distance (km)
B
SSE
CAYH
PIGN
STRA
NNW
C
S
MEND
GGIL
N
D
S
JACM
JAKH
LGNH
ARCH
DROU
BOIS
N
E
W
MGOA
PETG
GRBO
E

712 **Figure 7:** Variations in elevation, Moho depth, and Vp/Vs ratio across Haiti. The elevation
713 exaggeration is x10. (A) SW-NW across the central and southern part of Haiti, (B) and (C)
714 SE-NW and SW-NE across the northern part of Haiti, (D) S-N across the West of the central
715 and southern part, and (E) W-E across the southern part of Haiti. The orientations of the
716 transects are shown on Figures 5 and 6.
717

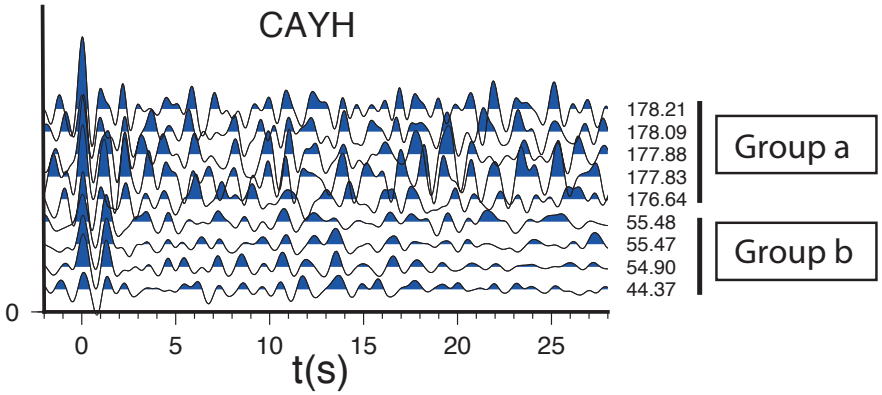
CAYH
178.21
178.09
177.88
177.83
176.64
Group a
55.48
55.47
54.90
44.37
Group b
0
0
5
10
15
20
25
t(s)

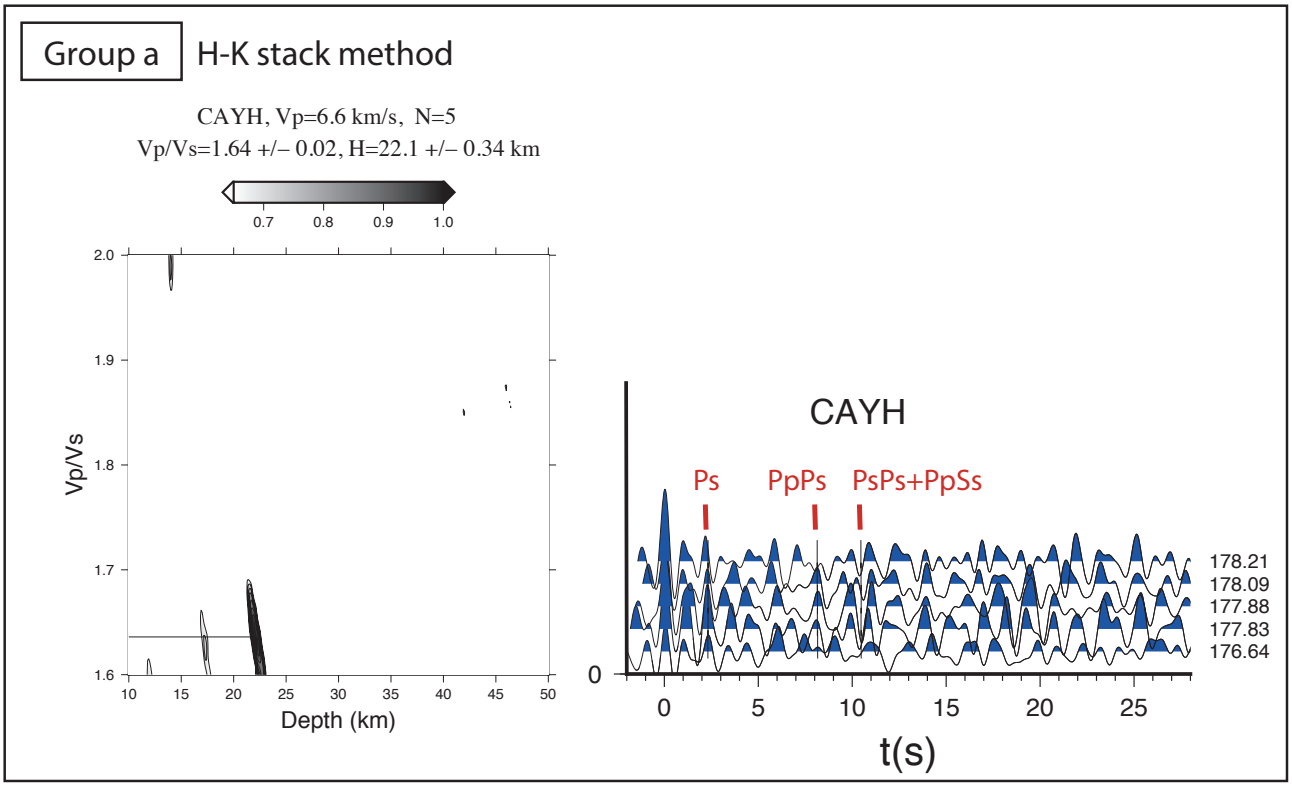
Group a
H-K stack method
CAYH, Vp=6.6 km/s, N=5
Vp/Vs=1.64 +/– 0.02, H=22.1 +/– 0.34 km
0.7
0.8
0.9
1.0
2.0
1.9
1.8
1.7
1.6
Vp/Vs
10
15
20
25
30
35
40
45
50
Depth (km)
CAYH
Ps
PpPs
PsPs+PpSs
178.21
178.09
177.88
177.83
176.64
0
0
5
10
15
20
25
t(s)

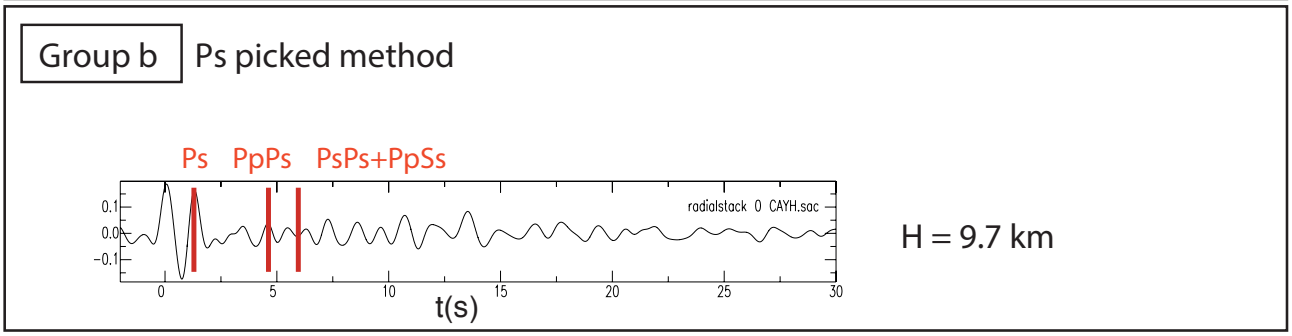
Group b
Ps picked method
Ps
PpPs
PsPs+PpSs
radialstack 0 CAYH.sac
0.1
0.0
-0.1
0
5
10
15
20
25
30
t(s)
H = 9.7 km

718

719

720

Figure 8: Estimation of the depth of an intracrustal layer for the station CAYH. The Moho depth is estimated at 22.1 km with Ps arrival and PpPs and PsPs+PpSs reverberations, using the H-K stack method and the RFs coming from the South (back-azimuth of about 170°, group a). A reverberation is imaged before the Ps arrival on RFs coming from the North-East (back-azimuth of about 55°, group b), and the corresponding estimated depth with Ps picked method (Vp=5.8 km/s and K=1.77) is 9.7 km.

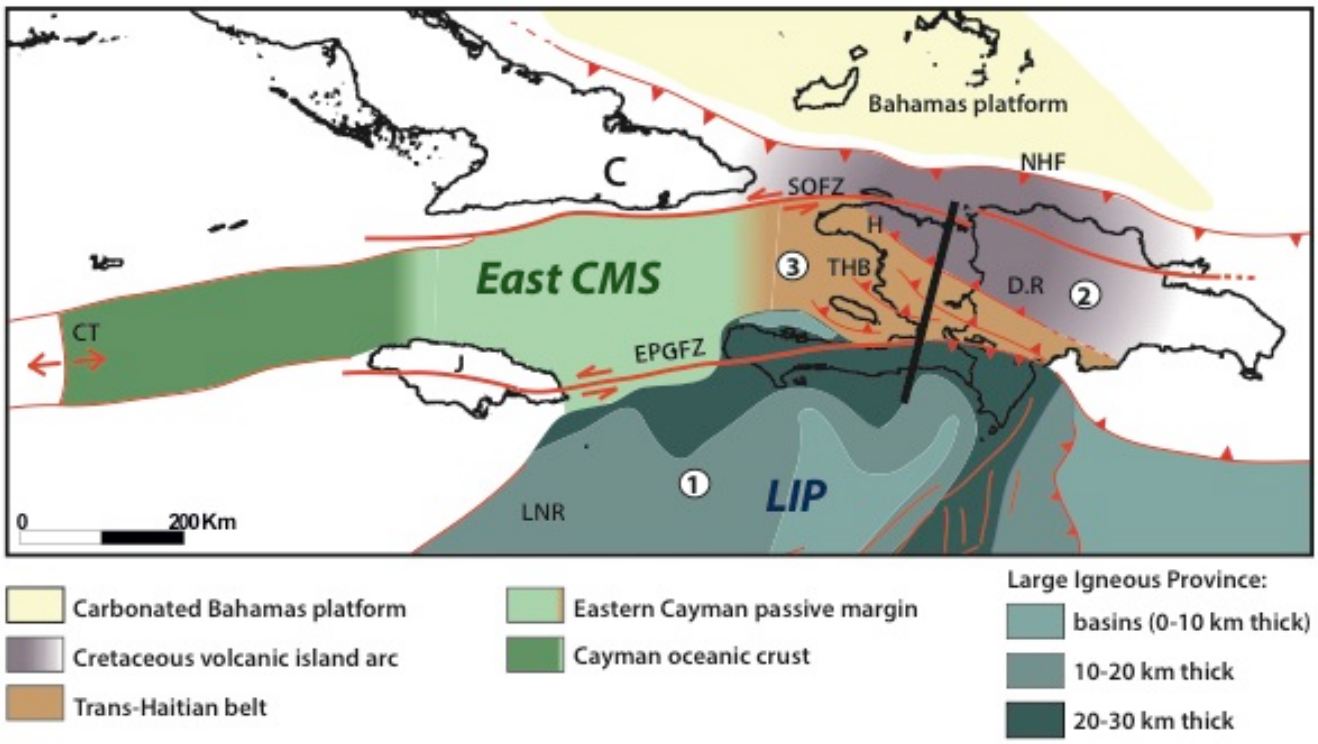

Figure 9: Location of the proposed different crustal domains we identified in Hispaniola. (1) the Caribbean Large Igneous Province, (2) the Cretaceous island arc and (3) the fold and thrust belt. C: Cuba; J: Jamaica; H: Haiti; D.R: Dominican Republic. NHF: North Haitian Fault; SOFZ: Septentrional-Oriente Fault Zone; THB: Trans-Haitian Belt; EPGFZ: Enriquillo-Plantain-Garden Fault Zone; CT: Cayman Trough; LNR: Lower Nicaraguan Rise. East CMS: eastern Cayman Trough margin system; LIP: Large Igneous Province. The black line indicates the localization of the transect shown in Fig. 10. The thicknesses of the LIP at sea are from Mauffret and Leroy (1997). The boundary between the East CMS and the LIP at sea is from Corbeau et al. (2016a).

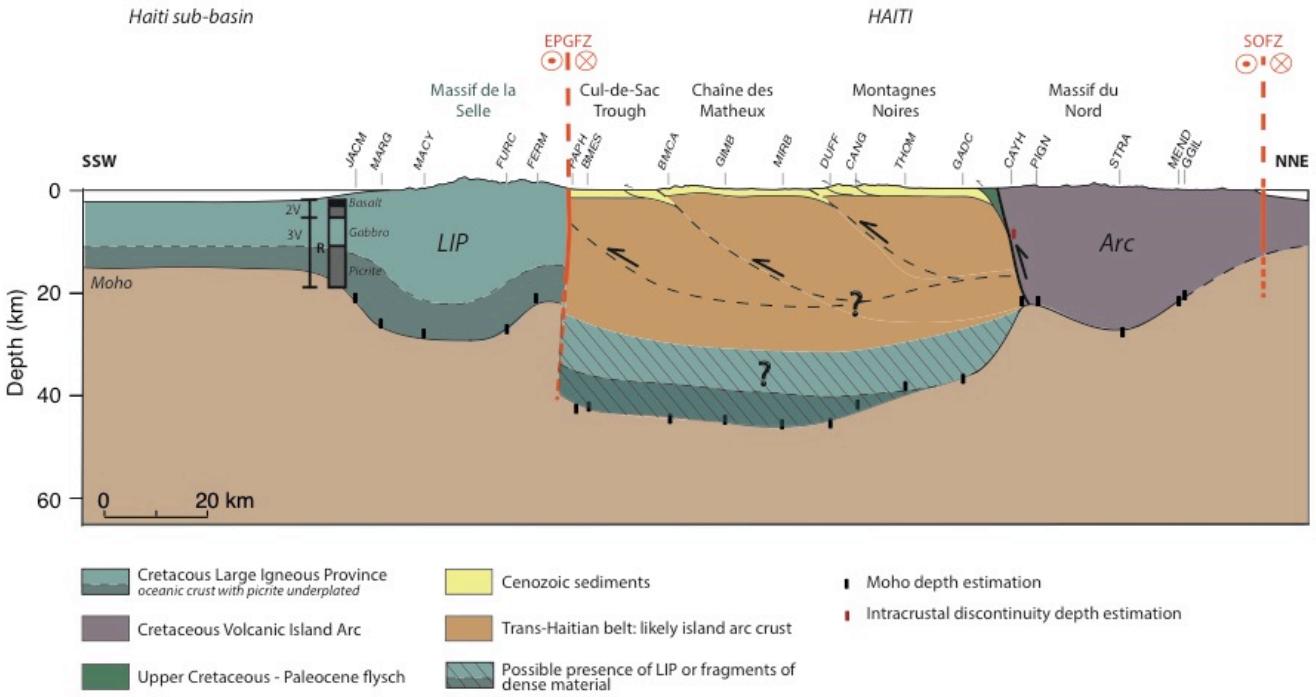

Figure 10: Summary conceptual geological transect across Haiti based on the Moho and intracrustal discontinuity depths. See Figs 2 and 9 for location of the profile. The seismologic stations are indicated. EPGFZ: Enriquillo-Plantain-Garden fault zone; SOFZ: Septentrional-Oriente fault zone. The log south of the transect is a model of the LIP crustal thickness based on a compilation of seismic refraction results: the layer 2V (original oceanic crust) is sandwiched between an upper basaltic layer (in black) and the layer 3V (original crust underplated); R is the top of a high velocity layer (Mauffret and Leroy, 1997).

Table 1: Moho depth (H) and Vp/Vs ratio (κ) estimated by the H-K stacking method

Stations	N	H(km)	δH(km)	K	δK
BMCA (line A)	13	44.3	0.1	1.98	0.01
BOIS (line D)	2	41.5	0.1	1.75	0.01
CANG (line A)	4	41.5	0.4	1.99	0.01
CAYH (line B)	5	22.1	0.4	1.64	0.02
CBOQ (line A)	7	39.5	0.7	1.82	0.02
DROU (line D)	7	47.2	0.4	1.85	0.02
DUFF (line A)	3	45.2	0.4	1.73	0.01
FERM (line A)	2	20.5	0.4	1.79	0.03
FURC (line A)	3	26.6	0.3	1.83	0.02
GGIL (line C)	3	20.1	0.7	1.81	0.04
GRBO (line E)	3	29.8	0.3	1.83	0.02
JACM (line D)	3	20.9	0.4	1.80	0.03
LGNH (line D)	8	34.6	0.4	1.96	0.02
MEND (line C)	6	22.5	0.4	1.94	0.02
MGOA (line E)	10	16.1	0.5	1.74	0.04
PETG (line E)	3	19.7	0.4	1.83	0.03
PIGN (line B)	4	22.1	0.5	1.86	0.04
STRA (line B)	4	28.2	0.4	1.67	0.03
THOM (line A)	5	37.9	0.5	1.87	0.02

Table 2: Moho depth (H) estimated by Ps picked method

Stations	N	H(km)	K
ARCH (line D)	5	32.3	1.80
BMES (line A)	5	41.9	1.80
GADC (line A)	4	36.4	1.85
GIMB (line A)	9	44.5	1.75
JAKH (line D)	9	19.0	1.80
MARG (line A)	3	25.5	1.80
MIRB (line A)	3	45.4	1.74
PAPH (line A)	9	42.3	1.85